PNAS | **June 11, 2002** | vol. 99 | no. 12 | **8009-8014**

Biophysics

Reduced-dimensionality NMR spectroscopy for high-throughput protein resonance assignment

Thomas Szyperski[*,†], Deok C. Yeh[*,‡], Dinesh K. Sukumaran[*], Hunter N. B. Moseley[§], and Gaetano T. Montelione[§]

[*] Departments of Chemistry and Structural Biology, State University of New York, Buffalo, NY 14260; and [§] Center for Advanced Biotechnology and Medicine, Department of Molecular Biology and Biochemistry, Rutgers University, Piscataway, NJ 08854

Communicated by Herbert Hauptman, Hauptman-Woodward Medical Research Institute, Buffalo, NY, April 12, 2002 (received for review November 15, 2001)

Abstract

A suite of reduced-dimensionality ^{13}C,^{15}N,^{1}H-triple-resonance NMR experiments is presented for rapid and complete protein resonance assignment. Even when using short measurement times, these experiments allow one to retain the high spectral resolution required for efficient automated analysis. "Sampling limited" and "sensitivity limited" data collection regimes are defined, respectively, depending on whether the sampling of the indirect dimensions or the sensitivity of a multidimensional NMR experiments *per se* determines the minimally required measurement time. We show that reduced-dimensionality NMR spectroscopy is a powerful approach to avoid the "sampling limited regime"—i.e., a standard set of ten experiments proposed here allows one to effectively adapt minimal measurement times to sensitivity requirements. This is of particular interest in view of the greatly increased sensitivity of NMR spectrometers equipped with cryogenic probes. As a step toward fully automated analysis, the program AUTOASSIGN has been extended to provide sequential backbone and $^{13}C^{\beta}$ resonance assignments from these reduced-dimensionality NMR data.

Introduction

Rapid resonance assignment is a prerequisite for high-throughput (HTP) structure determination and structural genomics (1). The aims of structural genomics are to (*i*) explore the naturally occurring "protein fold space" and (*ii*) contribute to the characterization of function through the assignment of atomic-resolution three-dimensional (3D) structures to proteins. The ultimate goal is to provide one or more representative 3D structures for every structural domain family in nature. It is now generally acknowledged that NMR will play an important role in this endeavor (1). The resulting demand for HTP structure determination requires fast and automated NMR data collection and analysis protocols. This impetus for the development of new methods will have broad impact in the technological infrastructure for structural biology and molecular biophysics.

Two key objectives for NMR data collection can be identified. Firstly, the measurement time should be minimized so as to lower the cost per structure and relax the constraint that NMR samples need to be stable over long time periods. Secondly, automated analysis requires recording of a redundant set of NMR spectra each affording good resolution, while it is also desirable to keep the total number of spectra small to reduce complications due to interspectral variations of chemical shifts (2). This second objective can be addressed by maximizing the dimensionality of the spectra. However, the joint realization of the first and second objective is impeded by the large lower bounds for measurement times of four (or higher) dimensional NMR spectra arising from the independent sampling of three (or more) indirect dimensions.

We distinguish "sampling limited" and "sensitivity limited" data collection regimes, depending on whether the sampling of the indirect dimensions or the sensitivity of the multidimensional NMR experiments *per se* determines the minimally achievable measurement time. Because structure determinations rely on nearly complete shift assignments routinely obtained using ^{13}C,^{15}N,^{1}H-triple-resonance (TR) NMR (3), the development of techniques that avoid the sampling limited regime represents an important challenge. Reduced-dimensionality (RD) TR NMR experiments (4-7), designed for simultaneous frequency labeling of two spin types in a single indirect dimension, offer a viable strategy to circumvent sampling-limited recording of NMR spectra. RD NMR is based on a projection technique for reducing the spectral dimensionality: the chemical shifts of the projected dimension give rise to a cosine-modulation of the transfer amplitude, yielding peak doublets encoding n chemical shifts in an n-1 dimensional spectrum. Thus, for example, four-dimensional (4D) information can be obtained in a 3D experiment. This reduces the sampling requirements and the minimal measurement time by about an order of magnitude (7), which allows recording projected 4D experiments within a few hours while retaining maximal evolution times and thus a resolution routinely achieved in conventional 3D NMR spectra. Furthermore, axial coherences, arising from either incomplete polarization transfer or steady-state heteronuclear magnetization, can be observed as peaks located at the center of the doublets (6). This allows both the unambiguous assignment of multiple doublets with degenerate chemical shifts in the other dimensions and the identification of cross peak pairs by symmetrization of spectral strips about the position of the central peak. RD NMR experiments were the first designed to simultaneously recruit both ^{1}H and heteronuclear magnetization for signal detection (6), and RD two-spin coherence NMR spectroscopy (8) serves as a valuable radio-frequency (rf) pulse module for measurement of cross-correlated heteronuclear relaxation rates (9). Here we present a suite of nine RD TR NMR experiments (six of which are unique implementations) for

complete protein resonance assignment. To integrate the RD NMR technology for rapid assignment, we have, as a step toward fully automated analysis, extended the program AUTOASSIGN (10, 11) for the use of RD NMR spectra.

Materials and Methods

NMR measurements were performed at 25°C on a Varian Inova 600 spectrometer by using a 1-mM solution of $^{13}C/^{15}N$-labeled "Z-domain" of the 71-residue *Staphylococcal* protein A (12) in 90% H_2O/10% D_2O (20 mM K-PO_4; pH, 6.5). The protein's overall rotational correlation time obtained from polypeptide backbone ^{15}N $T_{1\rho}/T_1$ ratios (13) is 4.5 ns—i.e., within the range encountered for proteins from about 5 to 15 kDa.

Nine RD NMR experiments were used in conjunction with 3D HNNCACB (4-8, 14-17). Fig. 1 surveys their names and the correlated chemical shifts. In the nomenclature of the RD NMR experiments underlined letters indicate chemical shifts obtained in a common dimension. Fig. 2 displays peak patterns observed in the projected dimensions, and Fig. 6 (which is published as supporting information on the PNAS web site, www.pnas.org) depicts the magnetization transfer pathways. Three-dimensional $H^{\alpha/\beta}C^{\alpha/\beta}$(CO)NHN (6, 7) and HACA(CO)NHN yield *sequential* connectivities. Three-dimensional HNNCAHA (7), HNNCACB, and $H^{\alpha/\beta}C^{\alpha/\beta}$COHA provide *intra*residue connectivities, and 3D HNN(CO,CA) (5) offers both intraresidue $^1H^N$–$^{13}C^\alpha$ and sequential $^1H^N$–$^{13}C'$ connectivities. Three-dimensional HCCH-correlation spectroscopy (COSY) and total correlation spectroscopy (TOCSY) provide assignments of *aliphatic* side chains, whereas two-dimensional (2D) HBCB(CGCD)HD and ^1H-TOCSY-relayed HCH-COSY provide those of the *aromatic* spins. The NMR pulse schemes of the hitherto unpublished RD NMR experiments are provided in Figs. 7-12, which are published as supporting information on the PNAS web site. The maximal evolution times, as well as the resulting measurement times are given in Table 1. RD NMR experiments in which ^1H and ^{13}C are simultaneously observed in a projected dimension were acquired with virtually the same maximal evolution times in $t_1(^{13}C/^1H)$ to enable accurate matching of peak patterns (Fig. 2). For HNNCAHA and HNN(CO,CA), central peaks were derived from incomplete polarization transfer (6, 7). For others, ^{13}C magnetization present at the end of the refocusing period of the initial polarization transfer from ^1H to ^{13}C was recruited, which yields two subspectra containing the peak pairs and central peaks, respectively (Fig. 2). In view of potential peak overlap, proper setting of the radio-frequency (rf) carriers is crucial. In HNNCAHA, for example, this allows one to place central peaks, and up-field and down-field component of the peak pairs into separate spectral regions (7). When data are collected in this manner, peak overlap does not increase when compared with HNNCA.

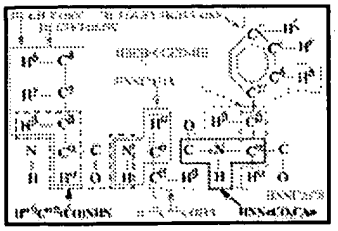

View larger version (31K):
[in this window]
[in a new window]

Fig. 1. Polypeptide chemical shifts correlated by the spectra constituting the standard set of experiments for RD NMR-based protein resonance assignment. The nuclei for which the chemical shifts are obtained from a given experiment are boxed and labeled accordingly. Experiments providing sequential and intraresidue connectivities are in black and gray, respectively.

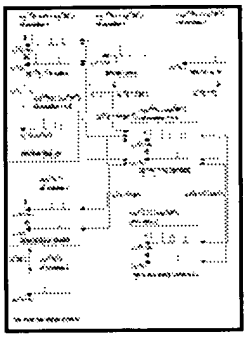

View larger version (27K):
[in this window]
[in a new window]

Fig. 2. Schematic presentation of the RD NMR-based HTP resonance assignment strategy by using the standard set of experiments of Fig. 1. The central role of 3D $H^{\alpha/\beta}C^{\alpha/\beta}$(CO)NHN is shown for establishing sequential connectivities via (*i*) $^{13}C^{\alpha}$ and $^{1}H^{\alpha}$ shift measurements (HNNCAHA, Fig. 3), (*ii*) $^{13}C^{\alpha}$ and $^{13}C^{\beta}$ shift measurements (HNNCACB), and (*iii*) $^{13}C{=}O$ shift measurements ($H^{\alpha/\beta}C^{\alpha/\beta}$COHA/HNNCAHA and HNN(CO,CA); see supporting information), as well as for assigning aliphatic (HCCH-COSY/TOCSY, Fig. 4) and aromatic side chains (HBCB(CGCD)HD and ^{1}H-TOCSY-relayed HCH-COSY, Fig. 5). Black double-headed arrows indicate connectivities that are established based on matching of peak patterns along ω_1($^{13}C/^{1}H$). Gray arrows indicate that the combined use of the two spectra requires the conversion of in-phase splittings into chemical shifts. Each box shows the peak patterns expected along ω_1, and the chemical shifts that are measured in the other dimensions are given above the corresponding boxes. Two cross sections are sketched for RD NMR experiments yielding two subspectra I and II, which comprise peak pairs and central peaks, respectively (6).

View this table:
[in this window]
[in a new window]

Table 1. Multidimensional NMR experiments

The relative sensitivity of NMR experiments was analyzed by determining the yield of peak detection—i.e., the ratio of observed peaks over the total number of expected peaks—and by separately assessing the S/N ratio distributions of peaks belonging to either peak pairs or central peaks. To rank the experiments (Table 1) according to sensitivity, only peaks encoding the prime information of a given spectrum were considered—e.g., *intra*residue connectivities in HNNCAHA and HNNCACB, correlation

peaks in HCCH-COSY and *relay* connectivities in HCCH-TOCSY. The averaged S/N ratios were divided by the square root of the measurement time (Table 1) and scaled relative to the most sensitive experiment yielding peak pairs—i.e., HACA(CO)NHN. To avoid a bias from longer transverse relaxation times in several flexibly disordered terminal residues, the N-terminal octapeptide segment comprising residues "−13" to "−6" (in the numbering chosen in ref. 12) was not considered in these sensitivity analyses.

The program AUTOASSIGN (V. 1.7.3; refs. 10 and 11) was extended for analysis of RD TR NMR experiments. The input included 3D peak lists derived from 3D HACA(CO)NHN, $H^{\alpha/\beta}C^{\alpha/\beta}$(CO)NHN and HNNCAHA, a 3D HNNCO peak list from 3D HNN(CO,CA) and the 3D HNNCACB peak list. Details of the computational protocol are available in *Supporting Text*, which is published as supporting information on the PNAS web site. The AUTOASSIGN program, the input RD NMR peak lists, and the output resonance assignment lists are available from the authors.

Results and Discussion

- Top
- Abstract
- Introduction
- Materials and Meth ds
- Results and Discussion
- Conclusion
- References

The data collection times and the relative sensitivities of the experiments are shown in Table 1. For those providing sequential connectivities—i.e., 3D HACA(CO)NHN, $H^{\alpha/\beta}C^{\alpha/\beta}$(CO)NHN, and HNN(CO,CA> (Fig. 1)—peak pair and central peak detection was complete (100%). Among the experiments providing *intra*residue connectivities, both 3D HNNCAHA and 3D HNNCACB likewise exhibited 100% yield, whereas a few were missing in $H^{\alpha/\beta}C^{\alpha/\beta}$COHA (yield, 98% of peak pairs; 91% of central peaks). In part, this is because magnetization is detected on the $^1H^{\alpha}$ protons close to the water resonance. Peak pair detection in 3D HCCH-COSY was nearly complete (90% of peak pairs, 93% of central peaks), whereas the yield of *relayed COSY* peak pairs in 3D HCCH-TOCSY was slightly lower (81%). To some extent this was due to signal overlap and not the lack of sensitivity. Nearly complete signal detection was also observed in 2D HBCB(CGCD)HD (100%) and ^{1}H-TOCSY-relayed HCH-COSY (90% of peak pairs). The detailed S/N analysis revealed (*i*) outstanding sensitivity for detection of peak pairs in 3D HACA(CO)NHN, (*ii*) about similar sensitivity for 3D $H^{\alpha/\beta}C^{\alpha/\beta}$(CO)NHN, HNNCAHA, HNN(CO,CA), HNNCACB (nowadays routinely used up to around 25 kDa), HCCH-COSY, and 2D ^{1}H-TOCSY-relayed HCH-COSY, and (*iii*) reduced sensitivity for 3D $H^{\alpha/\beta}C^{\alpha/\beta}$COHA, 2D HBCB(CGCD)HD, and relay peak detection in 3D HCCH-TOCSY. (Note that analysis of the spectra for assignment of the aromatic spin systems was somewhat impeded by the small number of aromatic residues in Z-domain, as well as their partially flexibly disordered nature.) In accordance with the very high sensitivity of HNNCO, central peak detection in HNN(CO,CA) is by far the most sensitive and serves for secure spin system identification in cases of overlap in 2D [^{15}N,^{1}H]-heteronuclear sequential quantum correlation (HSQC) (5, 10).

The analysis summarized in Table 1 allows one to devise a strategy for RD NMR-based HTP resonance assignment in which 3D $H^{\alpha/\beta}C^{\alpha/\beta}$(CO)NHN establishes sequential backbone connectivities and connectivities to both the aliphatic and aromatic side chains (Fig. 2). Firstly, the peak patterns along

$\omega_1(^{13}C^{\alpha/\beta}/^1H^{\alpha/\beta})$ in subspectra I and II of 3D $H^{\alpha/\beta}C^{\alpha/\beta}$(CO)NHN enable sequential resonance assignment in combination with HNNCAHA (Fig. 3) and HNNCACB, respectively. Complementary recording of 3D $H^{\alpha/\beta}C^{\alpha/\beta}$COHA and HNN(CO,CA) contributes polypeptide backbone $^{13}C'$ chemical shift measurements for establishing sequential assignments: the intraresidue $^{13}C'$ correlation is obtained by $\omega_1(^{13}C^{\alpha/\beta}/^1H^{\alpha/\beta})$ peak pattern matching of $H^{\alpha/\beta}C^{\alpha/\beta}$(CO)NHN with $H^{\alpha/\beta}C^{\alpha/\beta}$COHA, and the sequential $^{13}C'$ correlation is inferred from (13)C^α, ^{15}N, and $^1H^N$ chemical shifts in HNN(CO,CA) (see Fig. 7). Secondly, comparison of $\omega_1(^{13}C^{\alpha/\beta}/^1H^{\alpha/\beta})$ peak patterns with 3D HCCH-COSY and -TOCSY connects the $C^{\alpha/\beta}/H^{\alpha/\beta}$ chemical shifts with those of the more peripheral aliphatic side chain spins (Fig. 4), whereas comparison of $\omega_1(^{13}C^\beta/^1H^\beta)$ peaks with 2D HBCB(CGCD)HD and subsequent linking with $^1H^\delta$ chemical shifts detected in 2D ^{1}H-TOCSY-relayed HCH-COSY affords assignment of the aromatic spin systems (Fig. 5). For many residues the two β-proton chemical shifts are nondegenerate, and the connection of $H^{\alpha/\beta}C^{\alpha/\beta}$(CO)NHN with HBCB(CGCD)HD or HCCH-COSY/TOCSY may then rely on comparison of the three chemical shifts of $^1H^{\beta2}$, $^1H^{\beta3}$, and $^{13}C^\beta$. In general, the identification of peaks pairs is complicated when chemical shift degeneracy in the other dimension occurs, but central peak acquisition (Figs. 2 and 3) addresses this complication in a straightforward fashion (6). Importantly, however, pairs of peaks generated by a chemical shift in-phase splitting have quite similar intensity. Usually this does not hold for two arbitrarily selected peaks, because the nuclear spin relaxation times vary within each residue as well as along the polypeptide chain. The peak pairs are thus "labeled" with the relaxation times, making the pair identification obvious in most cases (Figs. 3-5). This is also advantageous for automated peak picking.

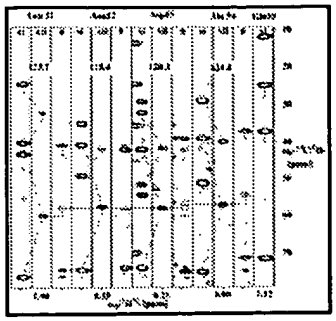

View larger version (35K):
[in this window]
[in a new window]

Fig. 3. Sequential resonance assignment from 3D $H^{\alpha/\beta}C^{\alpha/\beta}$(CO)NHN/3D HNNCAHA. Contour plots of [ω_1(^{13}C), ω_3($^1H^N$)]-strips taken from subspectrum I (strips labeled with AI) and subspectrum II (strips labeled with AII) of 3D $H^{\alpha/\beta}C^{\alpha/\beta}$(CO)NHN, and from 3D HNNCAHA (strips labeled with B) are shown. The strips were taken at the ^{15}N chemical shifts (indicated at the top) of residues 51 to 55 and are centered about their $^1H^N$ chemical shift. The sequence-specific resonance assignments of the amide chemical shifts are given at the top of each strip and are referred to as *i*. $\Omega(^1H^{\alpha/\beta}_{i-1})$ and $\Omega(^{13}C^{\alpha/\beta}_{i-1})$ obtained from 3D $H^{\alpha/\beta}C^{\alpha/\beta}$(CO)NHN are given in the strips AI and AII of residue *i*. Corresponding peak pairs in AI and central peaks in AII are connected by dashed lines, and sequential connectivities are indicated by solid lines for both peak pairs and central peaks. Dashed and solid contour lines represent negative and positive peaks, respectively, and sequential connectivities established via the central peaks and via the peak pairs are indicated by solid and dotted lines, respectively. Note that the near-degeneracy of $^{13}C^{\alpha}$ chemical shifts in the polypeptide segment Asn-52–Asp-53–Ala-54 is neatly resolved by the measurement of $^1H^{\alpha}$ chemical shifts encoded in the in-phase splittings of the peak pairs. Chemical shifts are relative to 2,2-dimethyl-2-silapentane-5-sulfonate (DSS).

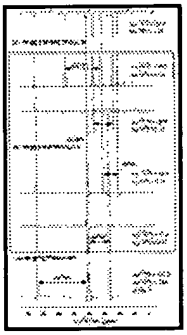

View larger version (26K):
[in this window]
[in a new window]

Fig. 4. Assignment of aliphatic spin systems exemplified for Lys-4. Cross sections were taken along ω_1(^{13}C/^{1}H) from the subspectra I comprising peak pairs of (*A*) 3D $H^{\alpha/\beta}C^{\alpha/\beta}$(CO)NHN, (*B*) 3D HCCH-COSY, and (*C*) 3D HCCH-TOCSY. The signals in 3D $H^{\alpha/\beta}C^{\alpha/\beta}$(CO)NHN were detected on the backbone amide proton of the succeeding residue Phe 5 (the ^{15}N and $^1H^N$ chemical shifts are indicated on the right). The cross sections taken from HCCH-COSY exhibit signals that were detected on $^1H^{\alpha}$, $^1H^{\beta}$, $^1H^{\gamma}$, and $^1H^{\delta}$ of Lys-4, respectively (from the bottom to the top), and the corresponding chemical shifts are given on the right. The in-phase splittings encode the $^1H^{\beta}$, $^1H^{\gamma}$, $^1H^{\delta}$, and $^1H^{\varepsilon}$ chemical shifts and serve to obtain the desired correlations (indicated by dashed vertical lines). Note that the peak signs vary because of aliasing along ω_2(^{13}C). In *C*, the signal was detected on $^1H^{\gamma}$ of Lys-4, and the crucial "CH–$^{\gamma}$CH-TOCSY *relay* connectivity is indicated. Chemical shifts are relative to 2,2-dimethyl-2-silapentane-5-sulfonate (DSS).

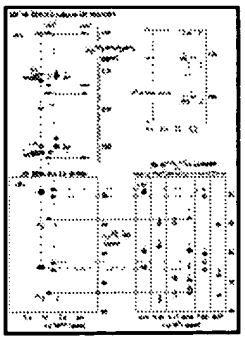

View larger version (29K):
[in this window]
[in a new window]

Fig. 5. Assignment of aromatic side chains exemplified for His(-4) and His-18, and Tyr-14. A composite plot of $[\omega_1(^{13}C/^1H),\omega_3(^1H^N)]$-strips taken from 3D $H^{\alpha/\beta}C^{\alpha/\beta}$(CO)NHN comprising the $\omega_1(^{13}C/^1H)$ peaks of all aromatic side chains in the polypeptide segment −5 to 58 of Z-domain, the 2D HBCB(CGCD)HD spectrum (*B*), and a spectral region taken from 2D ^{1}H-TOCSY-relayed HCH-COSY (*C*) are shown. The entire 2D ^{1}H-TOCSY-relayed HCH-COSY spectrum, which also contains cross peaks arising from $^{\varepsilon}$CH of the histidinyl residues, is shown in the upper right of the figure. Correlations belonging to His(-4) and His-18, and Tyr-14 are connected with long-dashed, dashed, and gray solid lines, respectively. In *C*, peaks arising from $^{\alpha}$CH moieties (which are not required for connecting the aromatic spin systems) are labeled with an asterisk. Chemical shifts are relative to 2,2-dimethyl-2-silapentane-5-sulfonate (DSS).

The suite of the nine experiments outlined in Fig. 1 complemented by 3D HACA(CO)NHN forms a "standard set" for RD NMR-based protein resonance assignment. For Z-domain, the entire set was recorded within only 65 h by using a conventional TR NMR probe at 600 MHz (Table 1). The high redundancy of these seven projected 4D, one conventional 3D, and two projected 3D spectra provides a very efficient resonance assignment strategy, which also profits from the fact that the detection of symmetric RD NMR peak pairs greatly facilitates the identification of peaks close to the noise level. Importantly, the information provided by projected 4D spectra cannot be obtained by recording twice the number of 3D spectra: in cases of chemical shift degeneracy a chemical shift quartuple is not equivalent to two shift triples.

It is of significant practical advantage that the sensitivity within the standard set varies only by about a factor of two (Table 1). This facilitates the prediction of minimal required measurement times (roughly a multiple of the measurement time of a single experiment). In fact, the S/N ratios observed in the first experiment allow one to adjust measurement times while data acquisition is in progress. For Z-domain, six RD NMR experiments were actually sufficient to provide complete backbone and side chain resonance assignments (3D $H^{\alpha/\beta}C^{\alpha/\beta}$(CO)NHN, HNNCAHA, HCCH-COSY/TOCSY, 2D HBCB(CGCD)HD, and ^{1}H-TOCSY-relayed HCH-COSY recorded in 36 h; Table 1), and those can be considered as a "minimal set" for proteins up to around 10 kDa. As expected, chemical shifts agreed well with those previously obtained at 30°C by using conventional TR NMR (12).

For proteins above ≈15 kDa, recording of highly sensitive 3D HACA(CO)NHN promises (*i*) to yield spin systems that escape detection in $H^{\alpha/\beta}C^{\alpha/\beta}$(CO)NHN, and (*ii*) to offer the efficient distinction of α- and β-moiety resonances by comparison with $H^{\alpha/\beta}C^{\alpha/\beta}$(CO)NHN. Moreover, Nietlispach *et al.* (18) have recorded 4D $H^{\alpha/\beta}C^{\alpha/\beta}$(CO)NHN for 50% random fractionally deuterated proteins reorienting with correlation times up to around 20 ns (corresponding to ≈20-30 kDa at ambient temperature). Thus, the 3D $H^{\alpha/\beta}C^{\alpha/\beta}$(CO)NHN, or a transverse relaxation optimized version thereof (19), may well maintain the role outlined in Fig. 2 for assigning partially deuterated proteins at least up to about that size, in particular

when using cryogenic probes (20).

Cryogenic probes reduce measurement times by about a factor of 10 or more (21). In the sensitivity-limited regime, where sampling requirements do not provide a bound for the minimal measurement time, the required signal could have been recorded for the standard set of ten experiments in about 6.5 h (Table 1). Using the current implementations (Table 1), the standard set could have been recorded with a single transient per increment and without central peak detection, considering the "spin relaxation time labeling" of peak pairs. This would then reduce the total measurement time to about 18 h. Hence, RD NMR promises to allow a rather close adjustment of measurement times to sensitivity requirements.

HTP employment of RD NMR requires strong computer support for data analysis. For the backbone and $^{13}C^{\beta}$ resonances, this issue was addressed by extending the program AUTOASSIGN (10, 11) to analyze 3D HACA(CO)NHN, $H^{\alpha/\beta}C^{\alpha/\beta}$(CO)NHN, HNNCAHA, HNN(CO,CA), and HNNCACB (recorded in 33 h; Table 1). AUTOASSIGN determined 94.5% (345 of 366) of all backbone $^{1}H^{N}$, ^{15}N, $^{13}C=O$, $^{13}C^{\alpha}$, $^{13}C^{\beta}$, and $^{1}H^{\alpha}$ chemical shifts with an error rate of only 0.9%, and obtained at least three chemical shifts for 61 of 63 residues (97%). Evidently, the good spectral resolution of the RD spectra (Table 1) greatly supported the efficient automated analysis. Importantly, the chemical shifts rapidly obtained from AUTOASSIGN directly revealed the protein's secondary structure (22): the helical boundaries derived independently from this chemical shift analysis and the NMR solution structure (12) are virtually identical. The extension of AUTOASSIGN for assigning side chain chemical shifts is currently in progress. This will allow one to automatically obtain nearly complete resonance assignments of proteins.

Conclusion

- Top
- Abstract
- Introduction
- Materials and Methods
- Results and Discussi n
- Conclusion
- References

RD NMR is a powerful approach to avoid the "sampling limited acquisition regime." This is of outstanding interest in view of the forthcoming era of cryogenic probes. In particular, the resulting rapid determination of protein secondary structure from chemical shifts (22) will greatly support fold prediction (23), protein target selection, and construct optimization in structural genomics. Considering that (*i*) sensitivity and sweep widths increase with increasing magnetic fields and that (*ii*) the widespread use of cryogenic probes will greatly boost the sensitivity of our spectrometers, we expect a "change in paradigm" in biological NMR spectroscopy with a new focus on research addressing the caveat of sampling limitation. Data processing protocols reducing the number of data points in the indirect dimensions without sacrificing spectral resolution, such as linear prediction and maximum entropy methods (24, 25), nonlinear sampling (25, 26), and possibly the recently introduced filter diagonalization method (27, 28), appear to be of keen interest to further enhance the impact of RD NMR.

Acknowledgements

This work was supported by a State University of New York start-up fund (to T.S.), National Science Foundation Grants MCB 0075773 (to T.S.) and DBI-9974200 (to H.N.B.M.), and National Institutes of Health (Northeast Structural Genomics Consortium) Grant P50 GM62413-01 (to T.S. and G.T.M.).

Abbreviations

HTP, high-throughput; RD, reduced-dimensionality; 2D, 3D, 4D, two-, three-, four-dimensional; COSY, correlation spectroscopy; TOCSY, total correlation spectroscopy; TR, triple-resonance; S/N, signal-to-noise.

Footnotes

† To whom reprint requests should be addressed at: Department of Chemistry, State University of New York, Buffalo, NY 14260. E-mail: szypersk@chem.buffalo.edu.

‡ Present address: Center for Advanced Research for Biotechnology, University of Maryland, Rockville, MD 20850.

References

▲ Top
▲ Abstract
▲ Introduction
▲ Materials and Methods
▲ Results and Discussion
▲ Conclusion
▪ References

1. Montelione, G. T. , Zheng, D. , Huang, Y. J. , Gunsalus, K. C. & Szyperski, T. (2000) *Nat. Struct. Biol.* **7**, 982-984[CrossRef][Medline].
2. Moseley, H. N. B. & Montelione, G. T. (2000) *Curr. Opin. Struct. Biol.* **9**, 635-642[CrossRef][ISI].
3. Cavanagh, J. , Fairbrother, W. J. , Palmer, A. G. & Skelton, N. J. (1996) *Protein NMR Spectroscopy* (Academic, San Diego).
4. Szyperski, T. , Wider, G. , Bushweller, J. H. & Wüthrich, K. (1993) *J. Am. Chem. Soc.* **115**, 9307-9308[ISI].
5. Szyperski, T. , Braun, D. , Fernández, C. , Bartels, C. & Wüthrich, K. (1995) *J. Magn. Reson. B* **108**, 197-203[CrossRef][ISI].
6. Szyperski, T. , Braun, D. , Banecki, B. & Wüthrich, K. (1996) *J. Am. Chem. Soc.* **118**, 8146-8147[CrossRef][ISI].
7. Szyperski, T. , Banecki, B. , Braun, D. & Glaser, R. W. (1998) *J. Biomol. NMR* **11**, 387-405[CrossRef][ISI].
8. Szyperski, T. , Wider, G. , Bushweller, J. H. & Wüthrich, K. (1993) *J. Biomol. NMR* **3**, 127-132[ISI][Medline].
9. Reif, B. , Hennig, M. & Griesinger, C. (1997) *Science* **276**, 1230-1233[Abstract/Free Full Text].

10. Zimmerman, D. E. , Kulikowski, C. A. , Huang, Y. , Feng, W. , Tashiro, M. , Shimotakahara, A. , Chien, C.-Y. , Powers, R. & Montelione, G. T. (1997) *J. Mol. Biol.* **269**, 592-610[CrossRef][ISI][Medline].
11. Moseley, H. N. B. , Monleon, D. & Montelione, G. T. (2001) *Methods Enzymol.* **339**, 91-108[ISI][Medline].
12. Tashiro, M. , Tejero, R. , Zimmerman, D. E. , Celda, B. , Nilsson, B. & Montelione, G. T. (1997) *J. Mol. Biol.* **272**, 573-590[CrossRef][ISI][Medline].
13. Szyperski, T. , Luginbühl, P. , Otting, G. , Güntert, P. & Wüthrich, K. (1993) *J. Biomol. NMR* **3**, 151-164[ISI][Medline].
14. Wittekind, M. & Müller, L. (1993) *J. Magn. Reson. B* **101**, 201-205[CrossRef][ISI].
15. Kay, L. E. (1993) *J. Am. Chem. Soc.* **115**, 2055-2057[ISI].
16. Yamazaki, T. , Forman-Kay, J. D. & Kay, L. E. (1993) *J. Am. Chem. Soc.* **115**, 11054-11055[ISI].
17. Zerbe, O. , Szyperski, T. , Ottiger, M. & Wüthrich, K. (1996) *J. Biomol. NMR* 7, 99-106[ISI].
18. Nietlispach, D. , Clowes, R. T. , Broadhurst, R. W. , Ito, Y. , Keeler, J. , Kelly, M. , Ashurst, J. , Oschkinat, H. , Domaille, P. J. & Laue, E. D. (1996) *J. Am. Chem. Soc.* **118**, 407-415[CrossRef][ISI].
19. Pervushin, K. , Riek, R. , Wider, G. & Wüthrich, K. (1997) *Proc. Natl. Acad. Sci. USA* **94**, 12366-12371[Abstract/Free Full Text].
20. Styles, P. , Soffe, N. F. , Scott, C. A. , Cragg, D. A. , White, D. J. & White, P. C. (1984) *J. Magn. Reson.* **60**, 397-404[ISI].
21. Monleon, D., Colson, K., Moseley, H. N. B., Anklin, C., Oswald, R., Szyperski, T. & Montelione, G. T. (2002) *J. Struct. Funct. Genom.*, in press.
22. Wishart, D. S. , Sykes, B. D. & Richards, F. M. (1992) *Biochemistry* **18**, 1647-1651.
23. Ortiz, A. R. , Kolinski, A. & Skolnick, J. (1998) *J. Mol. Biol.* **277**, 419-448[CrossRef][ISI][Medline].
24. Stephenson, D. S. (1988) *Prog. NMR Spectroscopy* **20**, 515-626.
25. Hoch, J. C. & Stern, A. S. (1996) *NMR Data Processing* (Wiley-Liss, New York).
26. Schmieder, P. , Stern, A. S. , Wagner, G. & Hoch, J. C. (1994) *J. Biomol. NMR* **4**, 483-490[ISI][Medline].
27. Wall, M. R. & Neuhauser, D. (1995) *J. Chem. Phys.* **112**, 8011-8022[CrossRef].
28. Hu, H. , Van, Q. N. , Mandelshtam, V. A. & Shaka, A. J. (1998) *J. Magn. Reson.* **134**, 76-87[CrossRef][ISI][Medline].

www.pnas.org/cgi/doi/10.1073/pnas.122224599

- Abstract of this Article (FREE)
- **Reprint (PDF) Version of this Article**
- Supporting Information
- Similar articles found in:
  - PNAS Online
  - ISI Web of Science
  - PubMed
- PubMed Citation
- Search PubMed for articles by:
  - Szyperski, T. || Montelione, G. T.
- Search for citing articles in:
  - ISI Web of Science (5)
- Alert me when:
  - new articles cite this article
- Download to Citation Manager

HOME HELP FEEDBACK SUBSCRIPTIONS ARCHIVE SEARCH TABLE OF CONTENTS

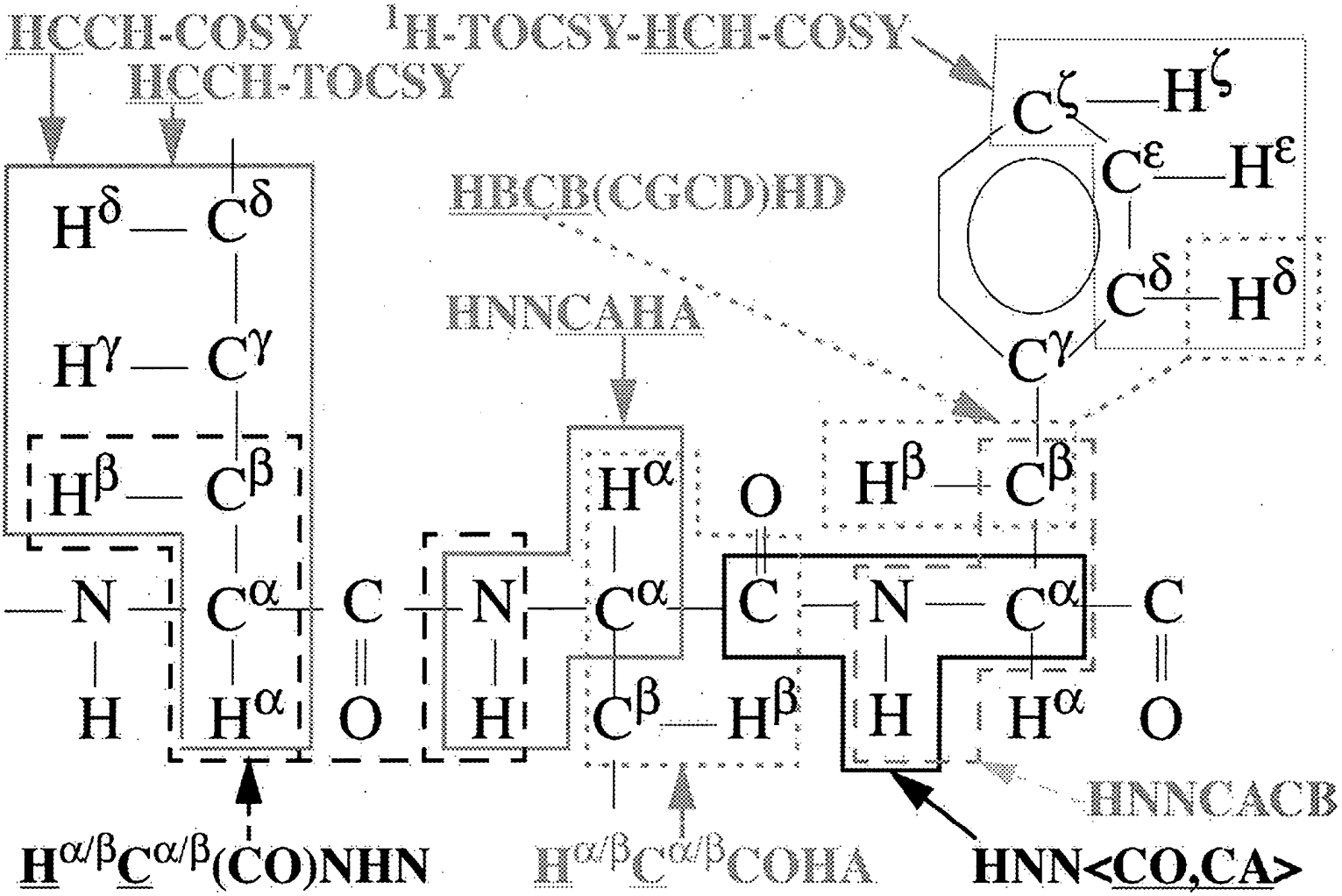
HCCH-COSY
HCCH-TOCSY
^{1}H-TOCSY-HCH-COSY
HBCB(CGCD)HD
HNNCAHA
HNNCACB
$H^{\alpha/\beta}C^{\alpha/\beta}$(CO)NHN
$H^{\alpha/\beta}C^{\alpha/\beta}$COHA
HNN<CO,CA>

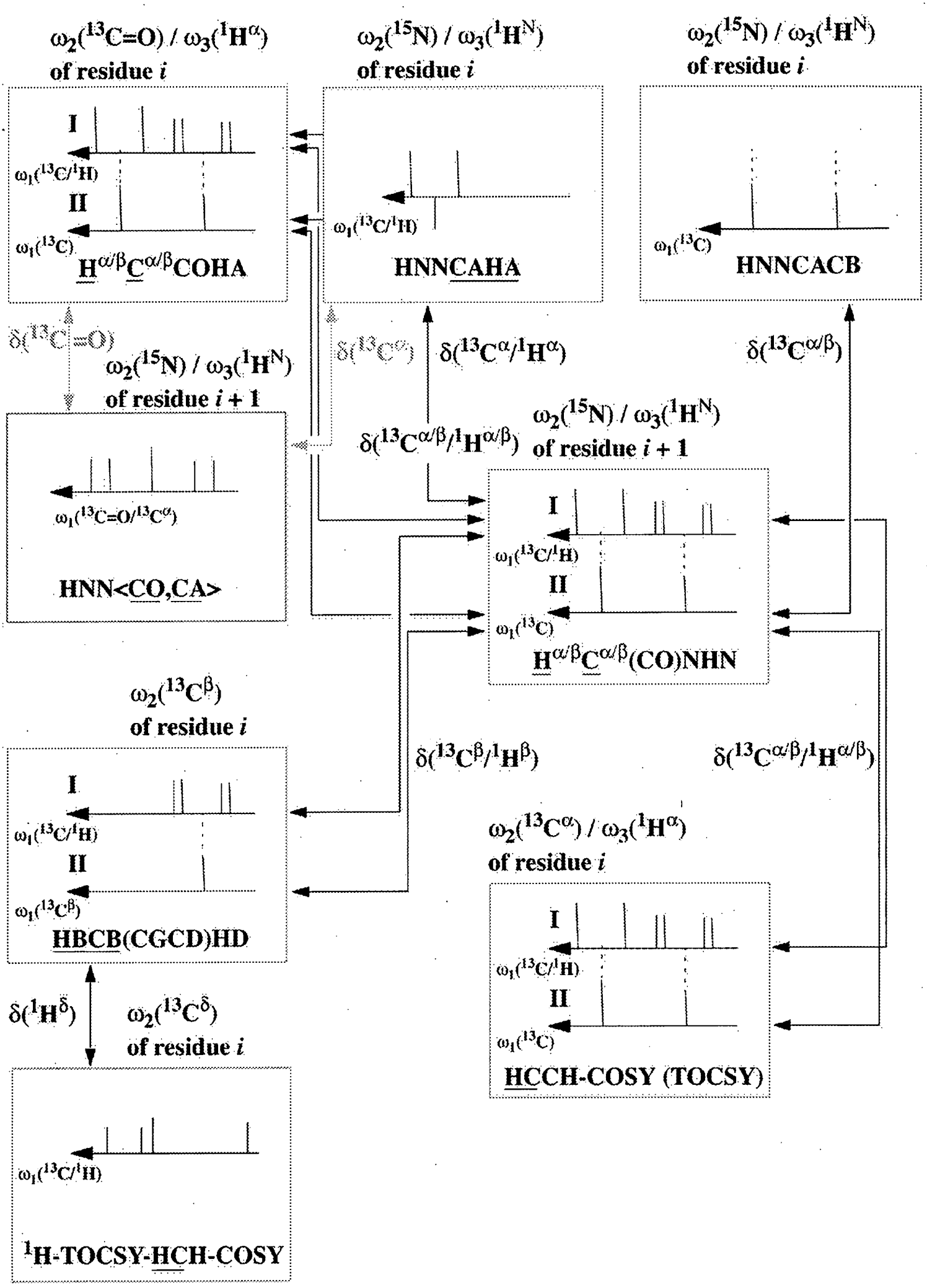
ω2(13C=O) / ω3(1Hα) of residue i
ω2(15N) / ω3(1HN) of residue i
ω2(15N) / ω3(1HN) of residue i
I
ω1(13C/1H)
II
ω1(13C)
Hα/βCα/βCOHA
ω1(13C/1H)
HNNCAHA
ω1(13C)
HNNCACB
δ(13C=O)
ω2(15N) / ω3(1HN) of residue i + 1
δ(13Cα)
δ(13Cα/1Hα)
δ(13Cα/β)
ω1(13C=O/13Cα)
HNN<CO,CA>
δ(13Cα/β/1Hα/β)
ω2(15N) / ω3(1HN) of residue i + 1
I
ω1(13C/1H)
II
ω1(13C)
Hα/βCα/β(CO)NHN
ω2(13Cβ) of residue i
δ(13Cβ/1Hβ)
δ(13Cα/β/1Hα/β)
I
ω1(13C/1H)
II
ω1(13Cβ)
HBCB(CGCD)HD
ω2(13Cα) / ω3(1Hα) of residue i
I
ω1(13C/1H)
II
ω1(13C)
HCCH-COSY (TOCSY)
δ(1Hδ)
ω2(13Cδ) of residue i
ω1(13C/1H)
1H-TOCSY-HCH-COSY